Deliverable

4.1. Pan-European remote sensing-assessment of drought impacts

Lars Eklundh, Hongxiao Jin, Zhanzhang Cai, Feng Tian

Department of Physical Geography and Ecosystem Science

Contents

1. Introduction

1.1 Drought

Climate change increases drought intensity, duration, and frequency in many regions of the world (IPCC 2021), which adversely affects societies (Van Loon *et al.* 2016) and ecosystems (Vicente-Serrano *et al.* 2020), increasing the importance of preparedness and knowledge of drought processes and impacts of climate variation. Drought reduces vegetation productivity (Ciais *et al.* 2005), increases tree mortality (Allen *et al.* 2010), alters vegetation composition (Pellizzari *et al.* 2017), and diminishes ecosystem services (Vicente-Serrano *et al.* 2020). In the European Union and the United Kingdom average drought losses during 1981 –2010 were about 9 billion euros per year (Naumann *et al.* 2021), half of which were agricultural losses (Cammalleri *et al.* 2020).

Drought development involves several related processes, starting with the so-called meteorological drought—a prolonged period of decreased precipitation (P) and/or increased atmospheric evaporative demand (AED), propagating to water depletion in soil, groundwater, rivers and reservoirs, and eventually causing plant water stress and affecting the socioeconomic situation in both developed and developing countries (Douville *et al.* 2021; Van Loon 2015). The accumulated difference between P and AED (P–AED, i.e. atmospheric water balance) over a specified period, the so-called Standardized Precipitation and Evapotranspiration Index (SPEI, Vicente-Serrano et al. 2010), has been used in many recent analyses of meteorological drought impacts on vegetation at global and regional scales (Christopoulou *et al.* 2021; Huang and Wang 2021; Lawal *et al.* 2021; Zhong *et al.* 2021). The average deviation of SPEI from normal depicts drought intensity, while the accumulated deviation depicts drought severity, following the drought terminology proposed by Dracup *et al.* (1980).

Ecological drought is the situation when vegetation is under water stress for a sustained period, impinging on ecosystem functions (IPCC 2021; Vicente-Serrano *et al.* 2020). Vegetation productivity is the biomass generated from carbon dioxide and water using solar energy, and drought impacts on vegetation productivity will affect all the subsequent ecosystem processes. Reductions in vegetation productivity, or eventually plant dieback, are direct plant responses to drought (Anderegg *et al.* 2012; Camarero *et al.* 2015; Choat *et al.* 2012; Marchin *et al.* 2022; McDowell *et al.*

2011; Senf *et al.* 2020). Indirect impacts include increased susceptibility to wildfire and biotic attacks (Allen *et al.* 2010; Hartmann *et al.* 2018; McDowell *et al.* 2008).

1.2 Plant responses to water stress

Plants in water-limited habitats have evolved to endure water stress through morphological, physiological, and biochemical adaptations, and have diverse strategies for responding to drought (Basu *et al.* 2016; Bohnert *et al.* 1995). For example, old leaves usually shed first in severe drought to allow fast recovery during rehydration (Pinheiro and Chaves 2010), indicating that plants have mechanisms to adjust leaf lifespan regarding water availability. Plant growth mechanisms and phenotypic plasticity increase the chances of survival during droughts (Bongers *et al.* 2017; Nicotra *et al.* 2010; Sánchez-Salguero *et al.* 2018). The growth plasticity is regulated by photosynthetic metabolism via plant hormones and signaling agents to promote plant protection and survival under stressful conditions (Baena-González *et al.* 2007; Cruz de Carvalho 2008; Shinozaki and Yamaguchi-Shinozaki 2006). Different genetic and molecular mechanisms of individual plant responses to drought may lead to coherent variations in primary production at the biome level.

The term *drought resistance* (or *drought tolerance*) is often used to describe the capability of plants to retain functioning under drought stress. However, to ecologists, drought resistance means survival, whereas to agronomists it means sustained crop yield or production retention. Plants in arid regions can often survive drought and are therefore drought-resistant from the ecologists' point of view. However, the production of these plants is vulnerable to drought, and they are hence drought-sensitive from an agronomists' or vegetation modelers' point of view (Ivits *et al.* 2016). Therefore drought resistance is an ambiguous term (Passioura 2002). Also, the rate of plant recovery, so-called *engineering resilience*, has been used to describe post-drought vegetation responses (Ivits *et al.* 2016; Lloret *et al.* 2011). The rate of post-drought plant recovery depends on many factors, such as drought severity and vegetation damage, vegetation type and age, phenology stage, drought-adaptation history, and post-drought environments, leading to unique recovery trajectories for individual plants (Folke 2006). It is therefore difficult to generalize at the ecosystem level. *Ecological resilience*, the capacity of vegetation to endure drought stress before a collapse, is a more suitable term for quantifying vegetation resilience to droughts over large scales and long periods (Holling and Meffe 1996). However, quantifying ecological resilience to drought is hampered

by a lack of thresholds beyond which the ecosystem collapse occurs. We here use the term *plasticity*, as an unambiguous descriptor of the capability of plants to change growth and productivity with water availability, both under drought stress and during post-drought recovery at individual or biome levels (Csermely 2015; Gray *et al.* 2021; Sánchez-Salguero *et al.* 2018).

1.3 Remote sensing of vegetation dynamics

Variations in plant growth and productivity can be sensed remotely from satellites (Myneni *et al.* 1997; West *et al.* 2019). For assessing vegetation status from satellite observations, several datasets and indices exist, for example, normalized difference vegetation index (NDVI), near-infrared reflectance of vegetation (NIRv), and many others (Ivits *et al.* 2014; Mishra and Singh 2010). Satellite-derived vegetation biophysical variables, such as leaf area index (LAI), fraction of absorbed photosynthetically active radiation (FPAR), solar-induced fluorescence (SIF) during photosynthesis, and gross primary productivity (GPP), are useful for inferring drought impacts on vegetation particularly over large spatial scales (e.g. Li and Xiao 2019; Running *et al.* 2004; Tagesson *et al.* 2021). The Plant Phenology Index (PPI, Jin and Eklundh 2014) is a robust indicator of photosynthetically active leaf area index, and is closely related to vegetation productivity (Abdi *et al.* 2019). PPI overcomes several limitations of other indices, including saturation in dense vegetation and signal biases from seasonal snow occurrence, an important characteristic in European alpine and high latitudinal biomes. PPI has been widely employed as an indicator for remotely sensed vegetation productivity of European biomes (EEA 2022; Tian *et al.* 2021).

1.4 European droughts

Europe has in general south-dry and north-wet conditions (Spinoni *et al.* 2017). The area of Europe experiencing water stress is projected to increase significantly by 2030, except for northern Europe (Strosser *et al.* 2012). However, also northern Europe has recently experienced very dry conditions, notably in 2018 (Junttila *et al.* 2023; Lindroth *et al.* 2020). Many European countries were facing the highest level of drought severity in the summer 2022 (Andrea *et al.* 2022), and multi-year severe droughts occurred in the first two decades of the 21st century (Büntgen *et al.* 2021; García-Herrera *et al.* 2019). These droughts greatly reduced vegetation productivity, as evident in eddy-covariance observations, crop yields, and ecosystem models for individual drought events. The reduction was highly heterogenous, depending on site, vegetation type, and drought intensity (e.g. Bastos *et al.*

2020; Ciais *et al.* 2005; Lindroth *et al.* 2020). At the pan-European level, several studies have synthesized vegetation responses to drought using remote sensing data. Ivits *et al.* (2016) showed that vegetation in northern Europe had weak and southern Europe had strong responses to droughts during 1982–2011. In particular, drought had minor impacts on boreal and alpine forests, but reduced productivity in agricultural areas significantly. Ivits *et al.* (2014) also found that vegetation productivity increased in northern and southern Europe but decreased in middle Europe during 1999–2010, with decreases attributed to drought impacts. Nevertheless, the issues of snow and dense vegetation in the employed proxies (Jin *et al.* 2017) together with coarse climate data resulted in difficulties quantifying drought impacts on vegetation productivity, leaving large areas unresolved (Ivits *et al.* 2014).

1.5 Objectives of this study

Here we report the use of improved high-resolution climate datasets and the novel satellite-derived proxy PPI for vegetation productivity to investigate the interannual variations of drought and vegetation productivity, and vegetation responses to drought across European biomes during 2000–2020. We use robust statistical methods to classify drought-vegetation associations, and attain robust regression estimates of slope from the time series, despite extreme values from drought events. We investigate how European drought is evolving, and how vegetation responds to drought across different European land cover types. We identify the regions and growth stages where plants display plastic or rigid responses to drought stresses to inform preparedness strategies for drought-vulnerable areas and seasons. A more comprehensive study of European vegetation response to drought using an ensemble of vegetation indicators (NDVI, NIRv, PPI, LAI, FPAR, SIF, and GPP) is still ongoing, and the results will be submitted for publication in a high-impact journal.

2. Data and methods

2.1 Study area

We focus on European biomes across a climate gradient from southern hot arid desert to northern cold humid tundra, covering latitudes 32.95°N to 73.55°N and longitudes 27.05°W to 45.05°E. Vegetated land cover was aggregated into seven major types: *non-irrigated cropland*, *irrigated cropland*, *grassland*, *broadleaf/mixed forest*, *needleleaf forest*, *shrubland*, and *wetland*, based on Corine Land Cover (CLC) 2018 (Version 2020_20u1, Figure 1a). The ESA (European Space Agency)

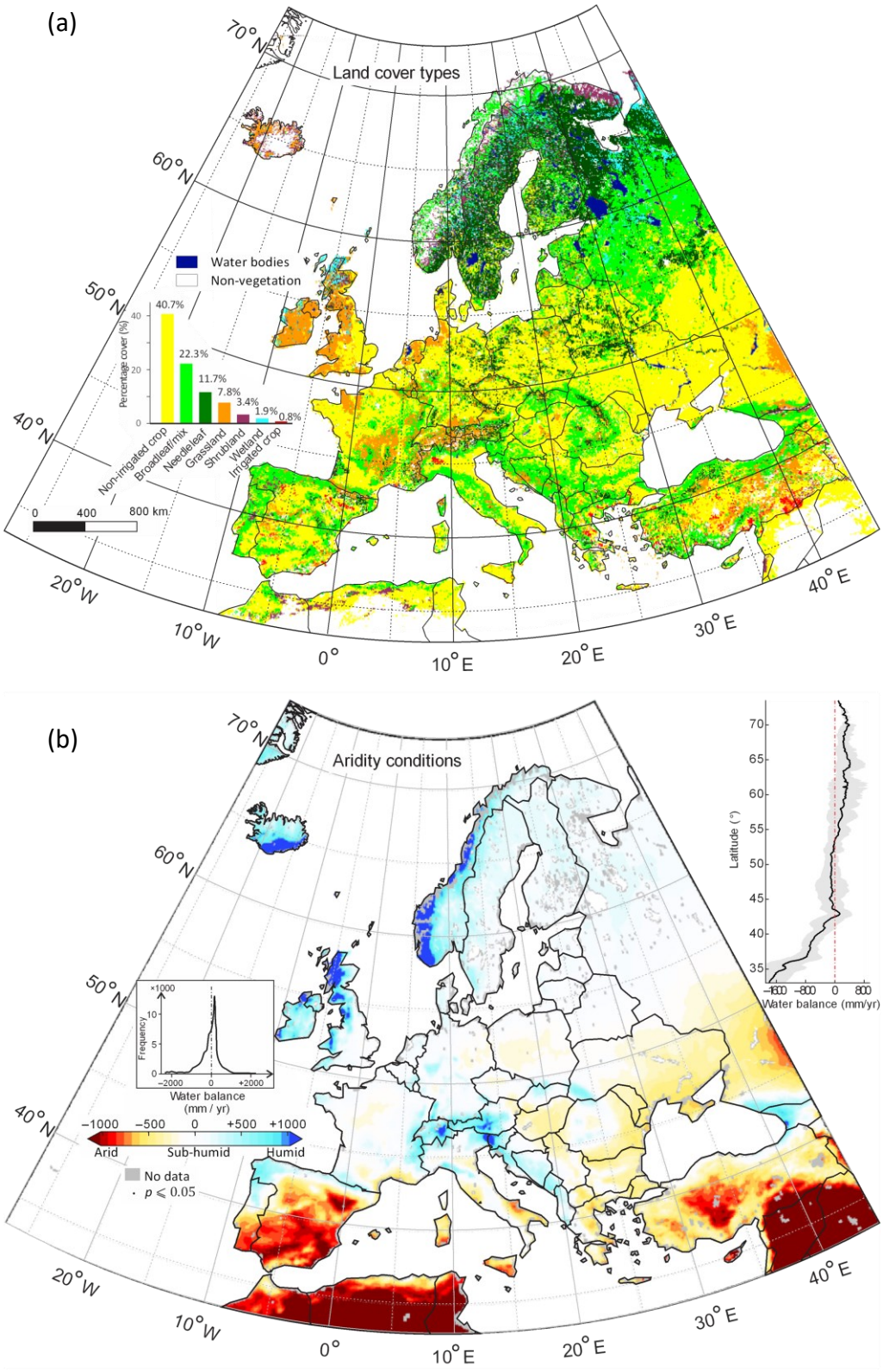

Figure 1. (a) Vegetated land cover types and (b) climatic aridity conditions of the study area. Vegetated land covers are aggregated into seven major classes based on the Corine Land Cover (CLC) 2018, and the ESA CCI land cover product 2020, with inset bar chart showing the legend and the percentage cover of the seven classes. Climatic aridity conditions are indicated by the mean annual water balance (P-AED) during 2000–2020, with insets show distribution frequencies and latitudinal profile.

Climate Change Initiative (CCI) land cover product of 2020 was used for regions outside CLC coverage. Both landcover datasets show good agreement, justifying their merging (Reinhart *et al.* 2021). To consider different physiological traits and agricultural management, and consequently differential drought responses, we separated croplands into irrigated and non-irrigated, and forests into broadleaf and needleleaf. Note that besides arable land, agricultural areas in CLC include pastures, vineyards, olive groves, and fruit and berry plantations (EEA 2021), all of which were aggregated to cropland in this study. The study area is dominated by non-irrigated cropland (40.7%), followed by broadleaf/mixed forest (22.3%), needleleaf forest (11.7%), and grassland (7.8%). The study area has climate conditions of south-dry, north and alpine mountains humid in general, indicated using the mean annual water balance during 2000–2020 (Figure 1b).

2.2 Climate data and drought index

Drought studies require accurate climate data with sufficient spatial resolution and coverage. Figure 2 shows that there are more than 30 datasets of precipitation currently available (Sun *et al.* 2018), of which we explored four widely used precipitation data sets.

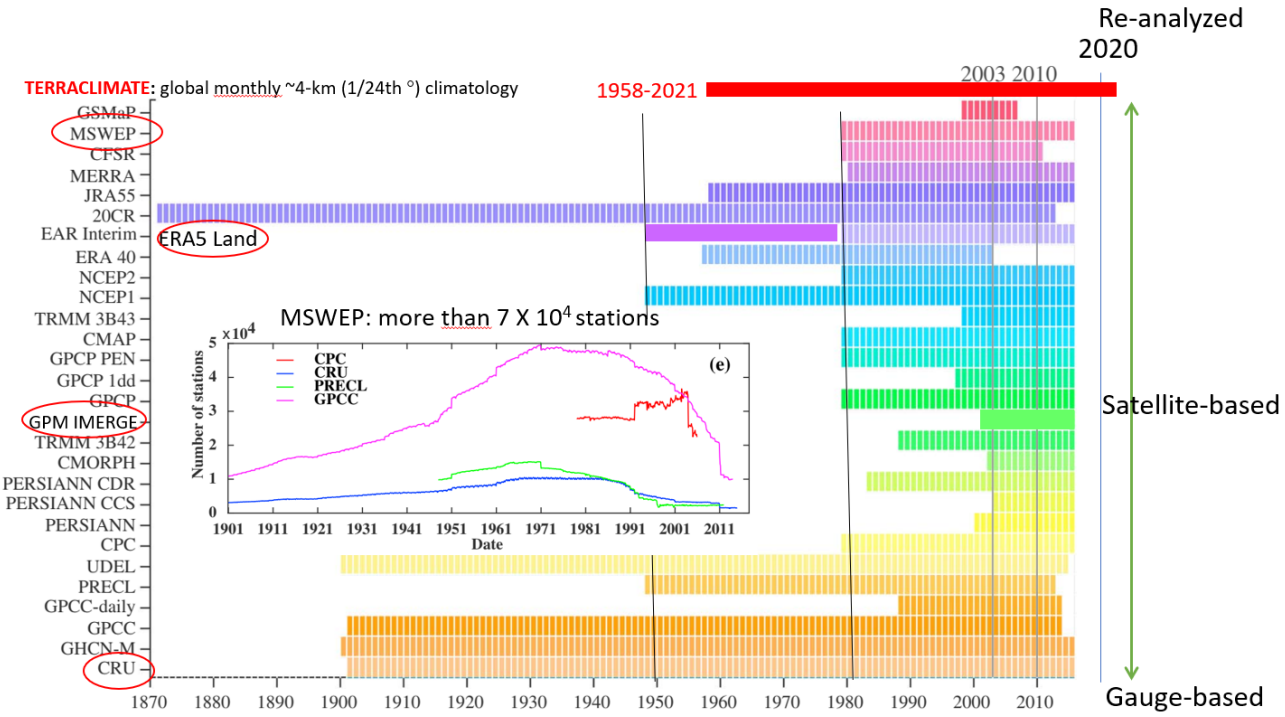

Figure 2. More than 30 datasets of precipitation available for drought study. Which one is the best in this project, in terms of accuracy, coverage, time span, spatial and temporal resolution? Modified from Sun et al. (2018).

2.2.1 CRU 4.05 precipitation

The CRU TS (Climatic Research Unit Timeseries) series of data sets contain monthly time series of precipitation, daily maximum and minimum temperatures, cloud cover, and other variables covering Earth's land areas for 1901-2020 (CRU TS4.05 is a recent release). The data set is based on analysis of over 4000 individual weather station records and gridded to 0.5°×0.5° resolution. Many of the input records have been homogenized and the data can be used for spatial analyses and trend studies together with other independent data sets.

2.2.2 GPM IMERG precipitation V06

NASA's Global Precipitation Measurement Mission (GPM) produces daily precipitation data using the Integrated Multi-satellite Retrievals for GPM (IMERG) over the majority of the Earth's surface by combining information from whatever constellation of satellites spanning 2000-2021 at 0.1°×0.1° resolution (V06) (V06, https://gpm1.gesdisc.eosdis.nasa.gov/data/GPM_L3/GPM_3IMERGDF.06/, Huffman *et al.* 2019).

2.2.3 Multi-Source Weighted-Ensemble Precipitation (MSWEP) Ver 2.1

MSWEP version 2.1 (released November 20, 2017) is a fully global, historic precipitation dataset (1979–2016) with a 3-hourly temporal and 0.1°×0.1° resolution. It takes advantage of the complementary strengths of gauge-, satellite-, and reanalysis-based data to provide reliable precipitation estimates over the entire globe. MSWEP has been validated at a global scale using observations from ~70,000 gauges and hydrological modeling for ~9000 catchments, with daily gauge corrections. MSWEP provides reliable global precipitation estimates by optimally merging rain gauge, satellite, and reanalysis data (Beck *et al.* 2019). More information on MSWEP, including links to technical details and information on downloading data, is available at http://www.gloh2o.org/.

2.2.4 ERA5-Land precipitation

The ECMWF ERA5-land dataset (https://www.ecmwf.int/en/era5-land) provides reanalyzed precipitation and other climatological data using the tiled European Centre for Medium-Range Weather Forecasts (ECMWF) Scheme for Surface Exchanges over Land incorporating land surface hydrology (H-TESSEL) available at 9 km × 9 km resolution with up to 3-hour temporal frequency during 1981–present (newly extended to 1950).

2.2.7 Drought index

Because of its ability to consider the joint contributions of temperature and precipitation to drought, and differentiate water deficiency at different time-scales, SPEI was used as a drought indicator in this study. SPEI has been shown to outperform other indices in evaluating drought impacts on soil moisture, vegetation activities, crop yield, and forest growth (Bachmair *et al.* 2018; Tian *et al.* 2018; Wang *et al.* 2016). We carefully compared precipitation from the above four resources and decided to use the Multi-Source Weighted-Ensemble Precipitation dataset considering its spatial resolution, period, and fidelity to gauge-based CRU data. The AED was calculated using climate variables from the ECMWF ERA5-land dataset (https://www.ecmwf.int/en/era5-land) following the FAO-56 Penman-Monteith equation (Allen *et al.* 1998). The accumulated water balance D was calculated as:

$$D_n^k = \sum_{i=0}^{2n-1} (P_{k-i} - AED_{k-i}), \qquad (1)$$

where *k* is the time position at a semimonthly time step, and *n* is the time-scale (n= 1, 2, …, 24 months). D was transformed to a normal distribution ***N***(0,1) using a 3-parameter log-logistic distribution to obtain SPEI for each semimonth-of-year and each time-scale over a reference period of 1981–2020, following Vicente-Serrano *et al.* (2010). We used semimonthly SPEI to investigate vegetation-drought associations across time-scales from 1 to 24 months, and then selected a time-scale of 3 months (SPEI3) for investigating vegetation responses to short-term drought impacts, and 12 months (SPEI12) for long-term drought, respectively, because a single SPEI time-scale could overlook vegetation responses to drought (Vicente-Serrano *et al.* 2013). We calculated drought intensity (SPEI average) during each vegetation growing season from semimonthly SPEI3 and SPEI12 to study interannual trends and extremes of droughts in European biomes during 2000–2020.

2.3 Vegetation productivity indicator

2.3.1 PPI data

PPI was used as an indicator of vegetation productivity. It was derived from the Moderate Resolution Imaging Spectroradiometer (MODIS) nadir bi-directional reflectance distribution function (BRDF) adjusted reflectance (NBAR) product (Version 6.0) at a daily time step and 0.05° spatial resolution:

$$PPI = -K \times ln(\frac{M-DVI}{DVI-0.09}), \quad (2)$$

where DVI is the difference vegetation index between red and near-infrared reflectance; M is the maximum DVI of each pixel during 2000–2020; and K is a factor calculated from M, solar zenith angle, and the diffuse fraction of radiation. PPI was calculated from daily data, then averaged at a semimonthly time step and upscaled to the 9km SPEI resolution for the European study area to investigate vegetation-drought associations. The growing season and the PPI sum were estimated using the TIMESAT software (Jönsson and Eklundh 2004), following Jin *et al.* (2019). PPI sum in the growing season was used as an indicator of annual vegetation productivity for assessing vegetation response to growing season drought intensity.

2.3.2 Other vegetation data

The following three vegetation variables, LAI, FPAR, and GPP, were directly downloaded from available resources.

LAI and FAPAR

The LAI and FPAR from 1999 to now are generated from three satellite platforms: SPOT/VGT, PROBA-V, and Sentinel-3, available from the Copernicus Global Land Service (CGLS) at 10-day interval and 1-km resolution with input data generated through VITO (http://www.vito-eodata.be). The VITO LAI and FPAR are publicly available at (https://land.copernicus.eu/global/products/fapar and LAI). Besides, considering the longer temporal coverage, we collected the Global Inventory Monitoring and Modelling System third generation (GIMMS3g) LAI covering 1982 to 2015 (Zhu *et al.* 2013).

GPP

We collected GPP data from two independent resources. One is GOSIF GPP, generated using the linear relationship between the global OCO-2-based SIF product (GOSIF) and flux tower GPP at a 0.05° spatial resolution and 8-day time step for the period from 2000 to 2020 (https://globalecology.unh.edu/data/GOSIF-GPP.html, Li and Xiao 2019). The other is the data generated from GIMMS 3g global semi-monthly normalized difference vegetation index (NDVI) using optimal light response function during photosynthetic carbon uptake (Tagesson *et al.* 2021). The data is publicly available at 1/12° spatial resolution for the period 1981 to 2015 (https://doi.org/10.17894/ucph.b2d7ebfb-c69c-4c97-bee7-562edde5ce66).

2.4 Data Analysis

2.4.1 Vegetation-drought correlation and classification

To investigate associations between drought and vegetation, the Spearman's rank correlation coefficients between time series of PPI and SPEI were calculated for drought time-scales from 1 to 24 months at a semimonthly timestep (24 annual timesteps) for the years 2000–2020. In total, 576 correlation coefficients (24 × 24) estimated for each 9 km × 9 km climate data pixel representing the European land surface (approx. 1.2×10^5 land pixels) were used to classify vegetation-drought associations. This was done by reducing the 576 dimensions to 3-D using the *t*-distributed stochastic neighbor embedding method (*t*-SNE, Maaten and Hinton 2008) and subsequently using a *k*-means method to generate initial clusters for the clustering of the correlation coefficient values using a Gaussian Mixture Model (GMM). Another widely used dimension reduction method, principal component analysis (PCA), was also explored but *t*-SNE performed better (see Figure S1).

Robust estimation of trends in vegetation and drought

Interannual trends in vegetation and drought for short record lengths (less than 30 years) may be estimated using a simple linear model:

$$PPI(t) = \alpha_{AV} + \beta_{AV} \cdot t + \varepsilon_{AV}(t), \quad (3)$$

$$SPEI(t) = \alpha_C + \beta_C \cdot t + \varepsilon_C(t), \quad (4)$$

where α and β are linear regression parameters for intercepts and trends. $\varepsilon(t)$ is the detrended time series of PPI or SPEI (residuals) that can be related to random events, like drought extremes.

AV and C represent Actual Vegetation and Climate respectively. A similar method for vegetation and drought trend estimation was used in Khoury and Coomes (2020), but modified here as follows. First, we computed the linear regression on an annual step using vegetation productivity and drought intensity for growing seasons, instead of pooling 12 months' data together. Second, we estimated robust trends using iteratively reweighted least-squares (Holland and Welsch, 1977) to reduce bias by extreme drought events, and therefore obtained robustly-detrended PPI and SPEI for drought event analysis.

2.4.2 Standardized anomalies of robustly-detrended vegetation and drought indicators

We analyzed drought events using standardized anomalies (SA) of robustly-detrended growing season PPI sums and mean SPEI values, i.e. the residual terms $\varepsilon(t)$ in (1) and (2):

$$SA(t) = \frac{\varepsilon(t)}{std(\varepsilon)}. \quad (5)$$

The anomalies are often represented as Z-scores of the time series (Deng *et al.* 2021; Horion *et al.* 2012). Here we particularly removed the trend in the Z-score calculation to deal with the non-stationary time series with an inconsistent mean. Drought-affected areas were defined by the pixels with SA$\leqslant$–1, either from PPI sums or mean SPEI values in the growing season.

2.4.3 Vegetation response to drought

Vegetation response to drought was estimated by including the drought variable in the linear regression (Khoury and Coomes 2020):

$$PPI(t) = \alpha_{PV} + \beta_{PV} \cdot t + \gamma \cdot SPEI(t) + \varepsilon_{PV}(t), \quad (6)$$

where β_{PV} is the potential vegetation trend without drought effects, and γ is the vegetation responsivity to drought. Positive γ indicates plastic plant response to drought—reducing productivity when drought intensity increases (SPEI decreases) and vice versa. Zero or negative γ indicates a rigid plant response to drought, disregarding meteorological drought stress.

The significance levels of regression slopes in (4) and (6) were estimated using a 2-tailed t-test. Both negative and positive SPEI were included in regression analysis to assess vegetation response to variations in drought intensity, instead of only variations in drier than normal conditions as reported in Ivits *et al.* (2016).

Meta-analysis of regression slope

The weighted least squares method (Becker and Wu 2007) was used to synthesize the overall robust regression slopes (responsivity γ or trend β) over an area of M pixels. Assuming regression slopes γ_i $(i = 1,2, \dots M)$ are independently and normally distributed:

$$\gamma_{meta} = \frac{\sum_{i=1}^{M} w_i \gamma_i}{\sum_{i=1}^{M} w_i}, \quad (7)$$

where the weight $w_i$is given by the reciprocal of slope variance: $w_i = 1/Var(\gamma_i)$. The significance level of the meta slope was estimated from the variance using the t-test. The statistical analysis was implemented using MATLAB (Ver 2020b, MathWorks, USA) statistics toolbox.

3. Results

3.1 Inter-annual variations in precipitation and drought

All four sets of precipitation data captured similar interannual variability of total precipitation over the entire European land, and therefore similar dry years and wet years from 2000 to 2020 (Figure 3), while the ERA5-land precipitation presented the highest absolution precipitation value among all datasets, with about 75% higher than that from CRU4.05 and MSWEP and 45% higher than GPM IMERG precipitation. During the past four decades (1981-2020), there was an overall increasing trend in annual total precipitation amount across European land, particularly since 2007, there were almost consistent positive precipitation anomalies in all four precipitation datasets (Figure 4). The increases in precipitation were most obvious in northern Europe above 65°N, whereas there was no interannual precipitation trend in central and southern Europe (below 65°N, Figure 4). Furthermore, the interannual variations in precipitation anomalies were large in the ERA5-land dataset, and small in CRU 4.05 and MSWEP datasets (Figure 4).

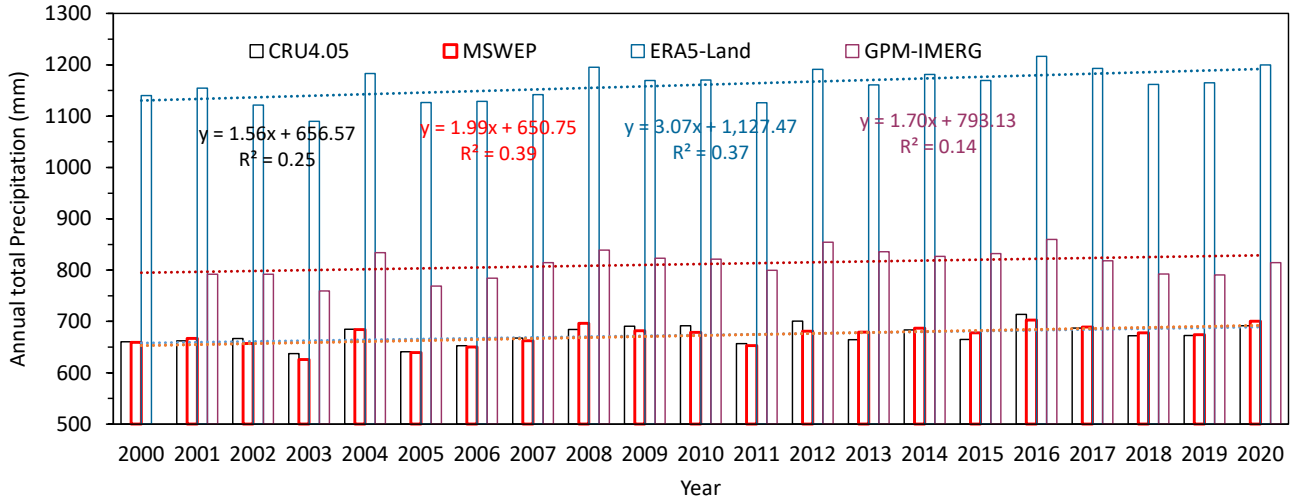

Figure 3. Comparison of annual total precipitation estimated from four datasets over entire European land, covering three main methods for estimating precipitation: gauge-based (CRU4.05), satellite-based (GPM-IMERG), and reanalyzed (ERA5-land and MSWEP). The re-analyzed precipitation from MSWEP shows high fidelity to gauge-based precipitation data CRU 4.05. The two analyzed data showed similar R2 in precipitation trends.

3.2 Spatial patterns of drought trends

Overall, the pan-European drought intensity in the growing season increased at a rate of 0.11 Z-score decade^{-1} for SPEI3 (p<0.001) and 0.14 Z-score decade^{-1} for SPEI12 (p<0.001) from the meta-analysis of regression slopes for entire Europe over the period 2000–2020 (Figure 5 and 6a). Over the study period. The drought intensity calculated using SPEI3 increased significantly in central European countries, western Russia, and Sweden, covering about 7.0% of the total land area (negative trends and $p \leqslant 0.05$, Figure 5a). The largest part (92.2%) of vegetated land areas show no significant drought trends. In contrast, drought intensity in the northern Mediterranean region, northern Ireland, and northwest Russia has weakened (positive trend), with 0.8% of the land area showing significant wetting trends ($p \leqslant 0.05$). Calculated using SPEI12, the area affected by increasing drought intensity is about 13.0% of the total land area, largely coinciding with the areas affected by 3-month time-scale droughts (Figure 5b). Western Russia, in particular, shows greater increasing drought intensity over the 12-month time-scale than the 3-month time-scale. Note that the drought trend differs from the average aridity conditions, i.e. the mean annual water balance (Figure 1b), which means that dry areas are not necessarily getting drier and moist areas moister, at least not in the last two decades.

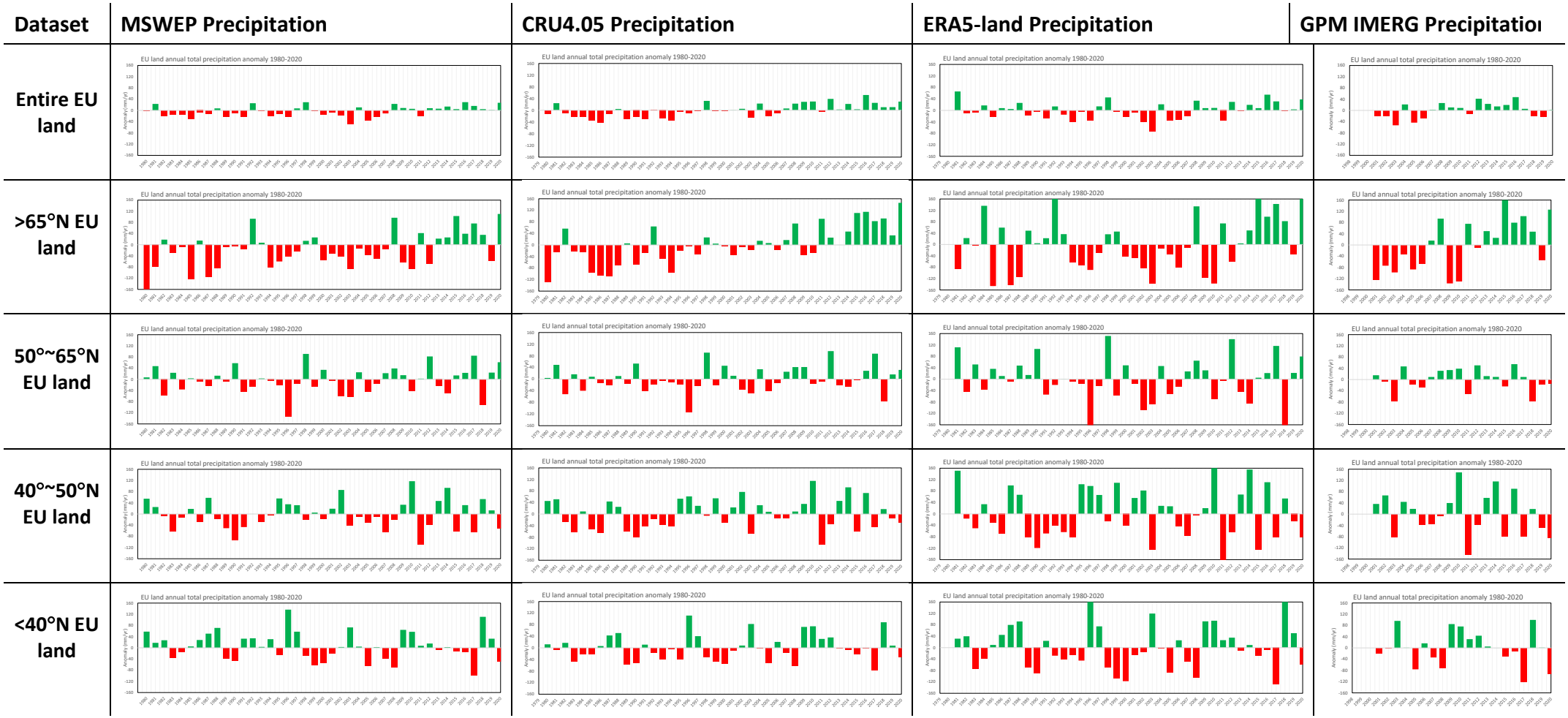

Figure 4. Comparison of the annual total precipitation anomalies over the entire European land and four latitudinal zones using four precipitation datasets: Multi-Source Weighted Ensemble Precipitation (MSWEP), Climatic Research Unit (CRU) 4.05, European Centre for Medium-Range Weather Forecasts (ECMWF) ERA5-Land, and Global Precipitation Measurement (GPM) IMERG. All data are in 0.1° spatial resolution except for CRU4.05 of 0.5° resolution. The MSWEP data has both high resolution and high fidelity to gauge-based CRU data, as well as more than 40 years of data available. Zoom in to see details in the e-version of the document.

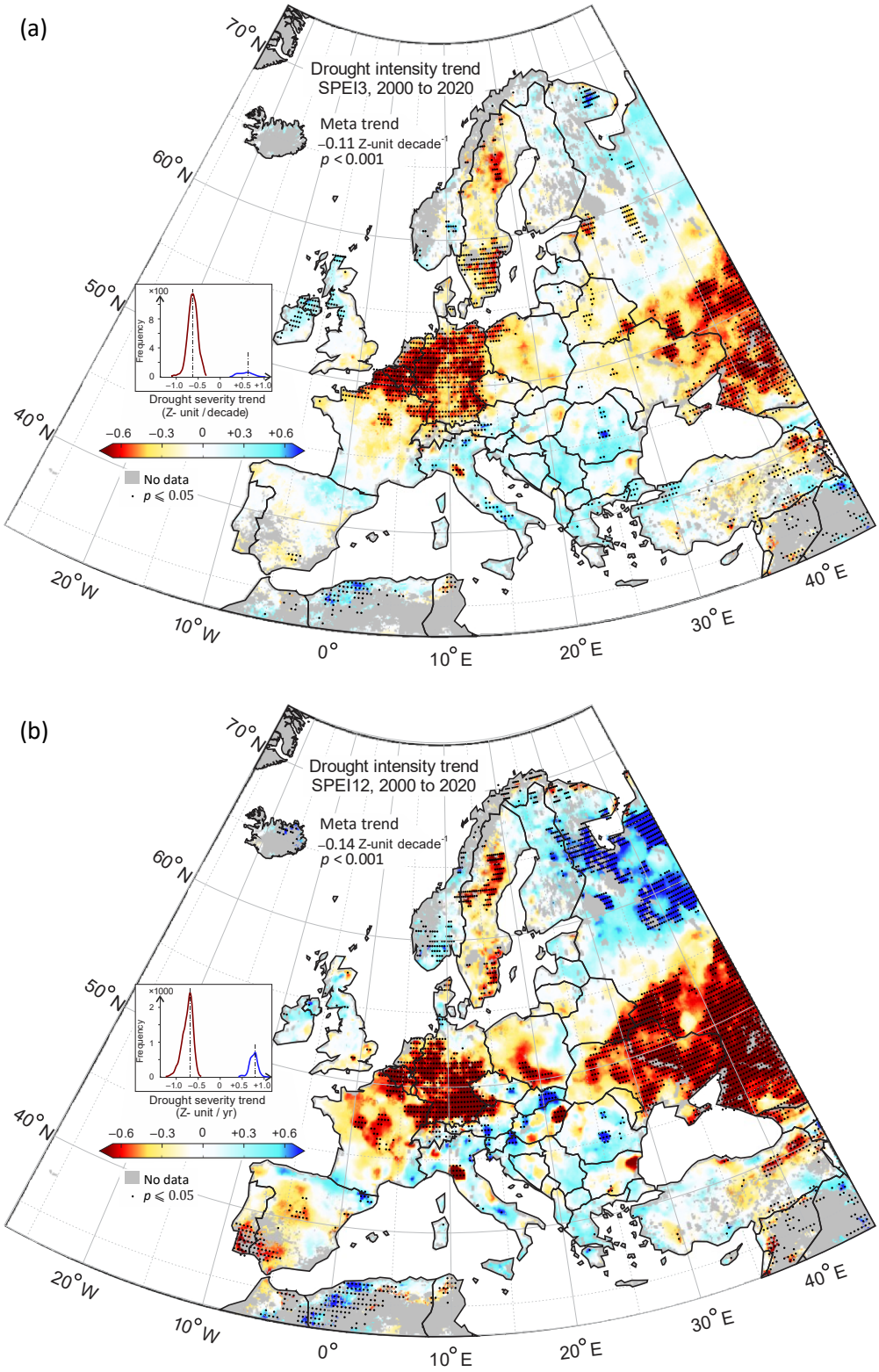

Figure 5. Trends of drought intensity estimated using average (a) SPEI3 and (b) SPEI12 in the growing seasons during 2000–2020. Inset histograms show frequencies in significant negative and positive values (p⩽0.05) respectively. The red color denotes the drying trend and the blue color denotes the wetting trend.

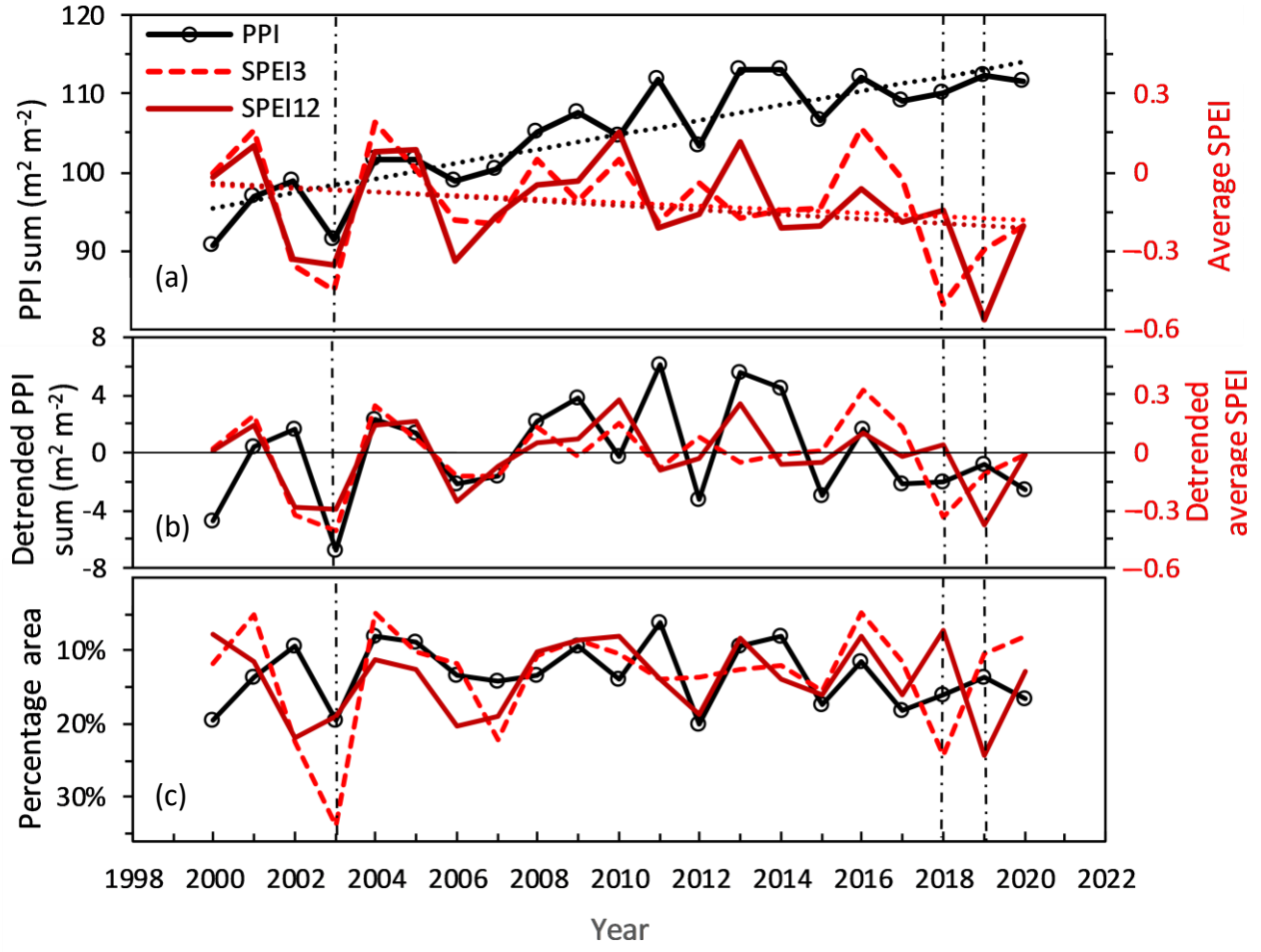

Figure 6. Interannual variations of (a) PPI growing season sums and average growing season SPEI3 and SPEI12, with dot lines indicating their trends estimated from meta-analysis of regression slopes that were from a robust algorithm of iteratively reweighted least-squares, (b) robustly-detrended time series of PPI and SPEI, and (c) percentage areas affected by drought in Europe determined using the standardized anomalies (SA) of PPI and SPEI3 and SPEI12 (SA$\leqslant$–1) respectively. Note the reversed y-axis in (c). Vertical dot-dash lines mark the extreme drought events in 2003 and 2018-19.

3.3 Inter-annual variations in vegetation growth

Vegetation productivity, as proxied by PPI sums, increased at an overall rate of about 6.4% per decade, or a meta trend (Eq. 7) of 6.7 m^2m^{-2} $decade^{-1}$, p<0.001 (Figure 6a and 7a). The overall potential vegetation growth rate could have reached up to 7.3% per decade (or 7.6 m^2m^{-2} $decade^{-1}$, p<0.001) if there had been no drying trend (Figure 7b). Hence, droughts slowed the vegetation productivity rate by up to 13.7% in Europe over the last two decades, albeit the absolute rate

reduction was merely 0.9 m^2m^{-2} $decade^{-1}$. Nonetheless, the increase in European vegetation productivity was strong enough so that individual drought impacts on vegetation are concealed. For example, the 2018 to 2019 drought impacts seemed trivial in the original PPI time series (Figure 6a), but were more noticeable after detrending (Figure 6b). The interannual variability in PPI sums co-varied weakly with the average growing season SPEI3 and SPEI12 in Figure 6b, but the correlations are insignificant (PPI-SPEI3: $r = 0.39$, $p = 0.20$; PPI-SPEI12: $r = 0.36$, $p = 0.11$).

Across European biomes, 38.2% of areas experienced a significant ($p \leqslant 0.05$) increase in vegetation productivity in the last two decades, with most of the highest growth rates in south-eastern Europe and the northern Mediterranean region. Only 2.3% of the land areas experienced a significant ($p \leqslant 0.05$) decrease in vegetation productivity, sporadically in Western European countries, such as France, Belgium, the UK, and Ireland (Figure 7a). Contrastingly, the European vegetation productivity significantly increased, although 41.4% of vegetated land areas were sensitive to short time-scale drought and 28.4% sensitive to long time-scale. This may be because, with the increasing temperature, the majority of the land area had no significant drought trends in Europe in the recent two decades. However, vegetation productivity could have increased more if there had been no increasing drought events in several European regions, especially in Germany, western Russia, and southern Sweden. Indeed, along with the decreased drought intensity in the northern Mediterranean regions, strong increases in vegetation productivity were observed. However, the vegetation productivity decreased in northern Ireland, but this might be due to other reasons than drought, since there was a wetting trend in the region.

The spatial variations of vegetation growth were solely based on daily PPI values at 500m resolution, an index used for indicating drought impacts on land vegetation by Europe Environment Agency (EEA https://www.eea.europa.eu/data-and-maps/data/data-viewers/drought-impact-on-ecosystems-in). The use of Plant Phenology Index (PPI) data offers significant benefits in tracking vegetation dynamics across various land covers, including the extensive evergreen boreal forests in the European landscape (Jin *et al.* 2019). Figure 8 compares PPI with other vegetation indicators, GPP, LAI, and FPAR generated from various satellite platforms and different algorithms. Overall, PPI effectively captured interannual variability of vegetation growth, providing strong evidence of PPI-derived vegetation response to droughts.

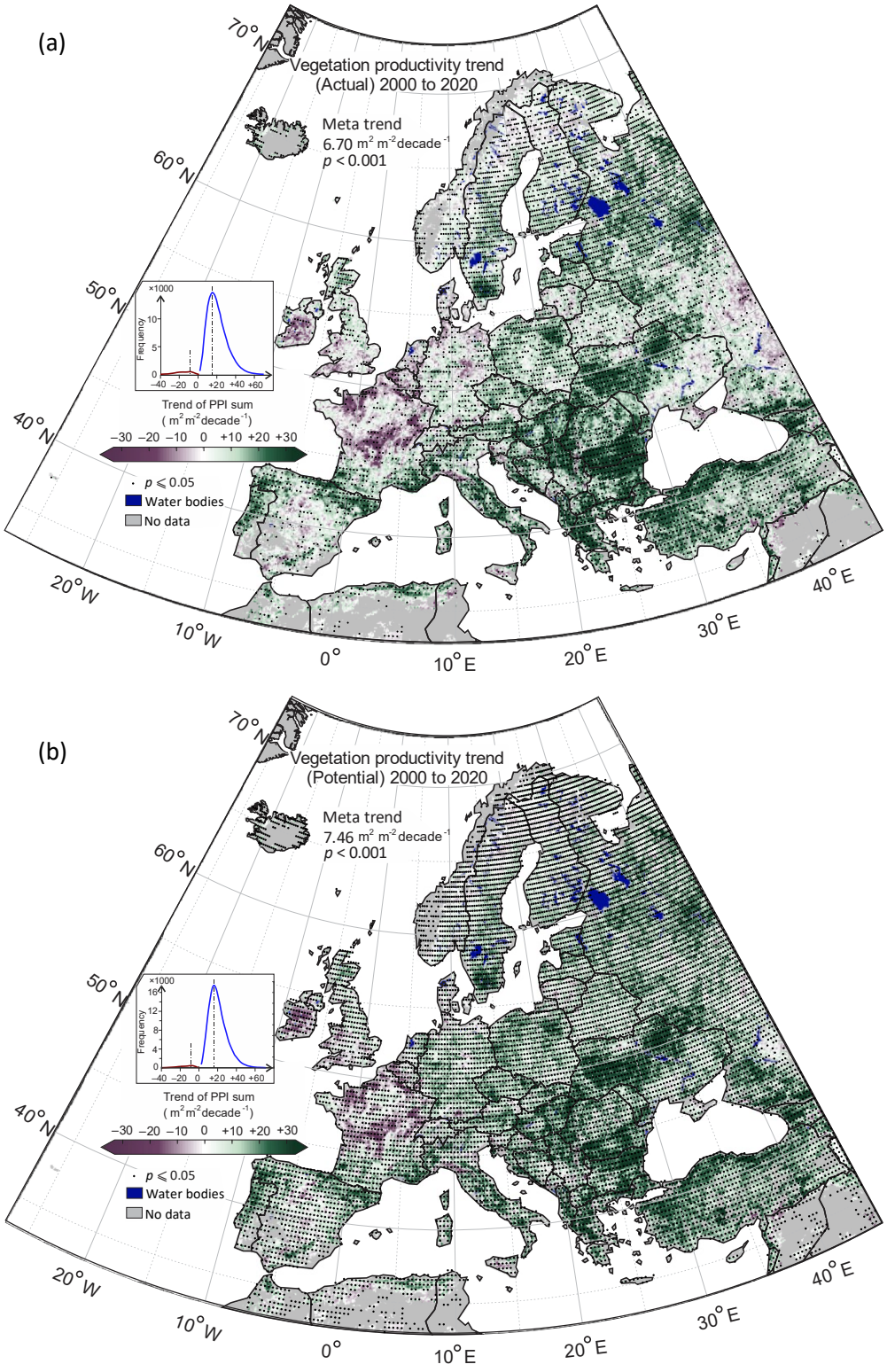

Figure 7. Map of vegetation growth trends in Europe from 2000 to 2020. (a) actual trends of annual total PPI, and (b) potential trends of annual total PPI if there had been no droughts (by controlling SPEI3). Inset histograms show frequencies in significant negative and positive values ($p \leqslant 0.05$) respectively. The green color denotes the increase in vegetation productivity and the purple decrease in productivity.

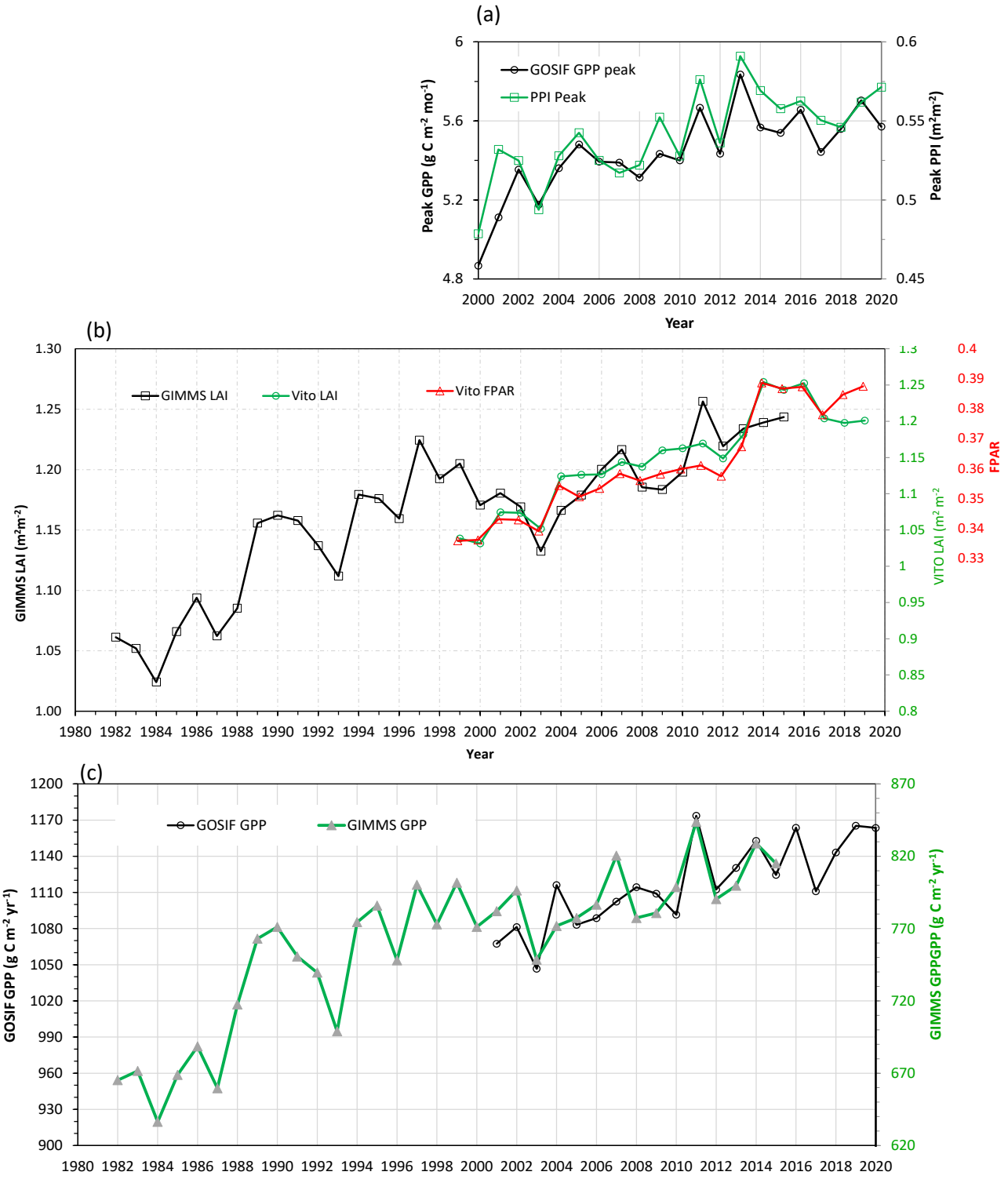

Figure 8. Time series of annual vegetation growth over entire Europe land, indicated using GPP, LAI, FPAR, and PPI. (a) Comparison of vegetation annual growing peaks estimated from PPI and GOSIF GPP respectively; (b) comparison of mean annual LAI (including GIMMS 3g data and ESA satellites' data processes by Vito) and FPAR (processed by Vito); and (c) comparison annual total GPP estimated from GOSIF data and GIMMS 3g NDVI data. There was an enhanced annual growth in European vegetation from 2000 to 2020 revealed in GPP, LAI, FPAR, and PPI.

3.4 Vegetation-drought responsivity and association

The weak correlation between PPI and SPEI is evident in the percentage of areas affected by drought, defined by the standardized anomalies (SA) of the two indicators, respectively (PPI-SPEI3: r = 0.32, p = 0.15; PPI-SPEI12: r = 0.15, p = 0.51, Figure 6c). Drought-affected areas determined using SPEI3 (SA$\leqslant$–1) are on average ~13.3% over the two decades, with a maximum of 33.9% in 2003. Using SPEI12, the average is about 13.8%, with a maximum of 24.2% in 2019. PPI revealed an average drought-impacted area of ~13.4%, with 19.6% and 13.5% of the area affected during 2003 and 2019, respectively. Overall, while similar average drought-affected areas are returned by PPI and SPEI, the interannual variations determined using PPI are smaller than those for SPEI, indicating that for large parts of Europe, the climate was more variable than vegetation. Figure 6 also reveals an apparent decoupling between vegetation growth (PPI), and drought at different time-scales (SPEI3, and SPEI12), in terms of drought intensity and affected areas in recent years, particularly since 2013. After 2013 the PPI sum leveled off, while the drying trend accelerated (Figure 6a).

Biomes over 41.4% of the vegetated area in Europe display a significant plastic response (positive responsivity and $p\leqslant0.05$) to drought using SPEI3 (Figure 9a). These areas are predominately located in central and southern Europe, 69.5% of which are croplands. Moldova in eastern Europe and the Massif Central in southern France show particularly strong responses to drought. When viewed over the long time-scale of 12 months (SPEI12), the fraction of drought-plastic areas partly coincided with the 3-month time-scale drought but was significantly smaller (28.4%, $p\leqslant0.05$, Figure 9b). Again, Moldova stands out as drought-responsive also in the long term. Both maps of drought responsivity using SPEI3 (Figure 9a) and SPEI12 (Figure 9b) show that northern biomes are rigid to drought (negative responsivity) and southern biomes (excluding mountainous and high plateau regions) are plastic to drought. Most areas in the UK and Ireland are plastic to drought at a 3-month time-scale (SPEI3) but do not respond to drought at a 12-month time-scale (SPEI12).

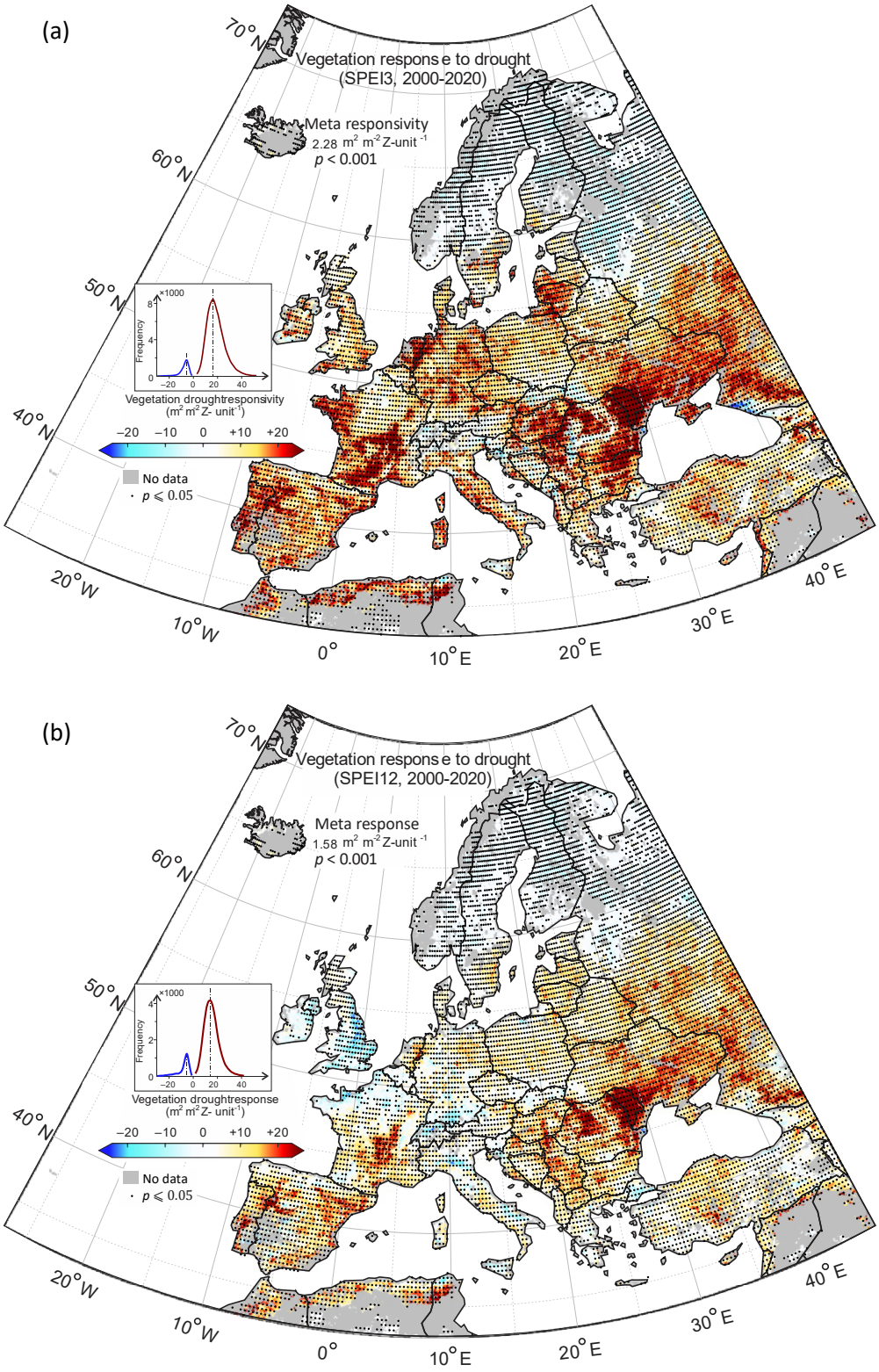

Figure 9. Vegetation responsivity to drought using PPI sum and (a) SPEI3 or (b) SPEI12. Inset histograms show frequencies in significant negative and positive values (p⩽0.05). Red color denotes vegetation plastic response to drought, and blue color denotes vegetation rigidity to drought.

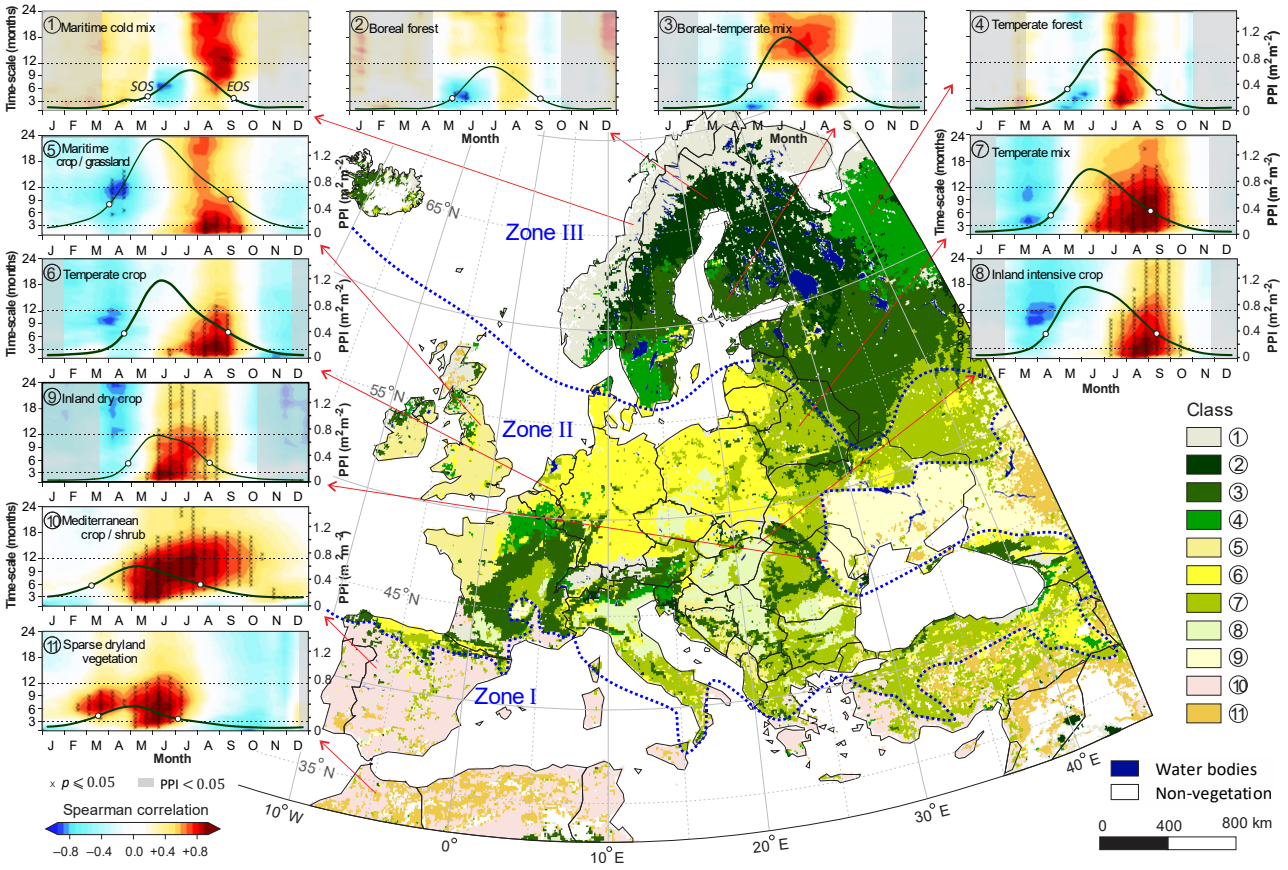

Figure 10. Map of drought-vegetation association classes in Europe. Inset figures show the median Spearman correlation of each class in time-scale-month plane with red color (positive correlation) indicating drought-plasticity, blue color (negative) drought-rigidity; "×" denotes correlation significant at $p \leqslant 0.05$; grey shaded area denotes no vegetation growth (PPI<0.05). Dominant time-scales with significant correlation are from 3 to 12 months. The black solid line in each inset figure denote the average seasonal PPI trajectories (solid line), and the black circle markers denote the start-of-season (SOS), and the end-of-season (EOS).

The statistical association between vegetation and drought across Europe is displayed in Figure 10. Vegetation productivity was correlated to drought at different phenological stages across European biomes. At each phenological stage, the correlation was either negative or positive (month-wise stripe pattern, Figure 10, insets) with varied strength across different accumulation periods (time-scales), with the majority of significant correlations occurring at time-scales of 3–12 months. Based on the month-time-scale pattern, the correlations were grouped by unsupervised classification into 11 vegetation-drought association classes using t-SNE dimension reduction and the GMM method (Figure 10): ① Marine cold mixed vegetation, ② Boreal forest, ③ Boreal-temperate mixed forest, ④ Temperate forest, ⑤ Maritime crop/grassland, ⑥ Temperate cropland, ⑦ Temperate mixed vegetation, ⑧ Inland intensive cropland, ⑨ Inland dry cropland, ⑩ Mediterranean

crop/shrubland, and ⑪ Sparse dryland vegetation. Classes ①–④ are dominated by forest land covers (broadleaf and needleleaf), and ⑤–⑪ by non-irrigated cropland cover (Figure S2).

Classes ① and ② are in cold regions, showing rigidity to drought extremes at 3 and 12-month time-scales (Figure 11), indicating that plants can maintain or even increase growth irrespective of SPEI reduction, but do not expose enhanced growth when water is abundant. Classes ③ and ④ are in mixed boreal-temperate regions, and central European highlands and alpine regions characterized by humid conditions, such as the Pyrenees, Massif Central, Alps, Carpathians, and the Caucasus. Cropland-dominated classes are mostly in central and southern Europe, and have diverse responsibilities to drought stress. Classes ⑥–⑪ have plasticities to both 3 and 12-month time-

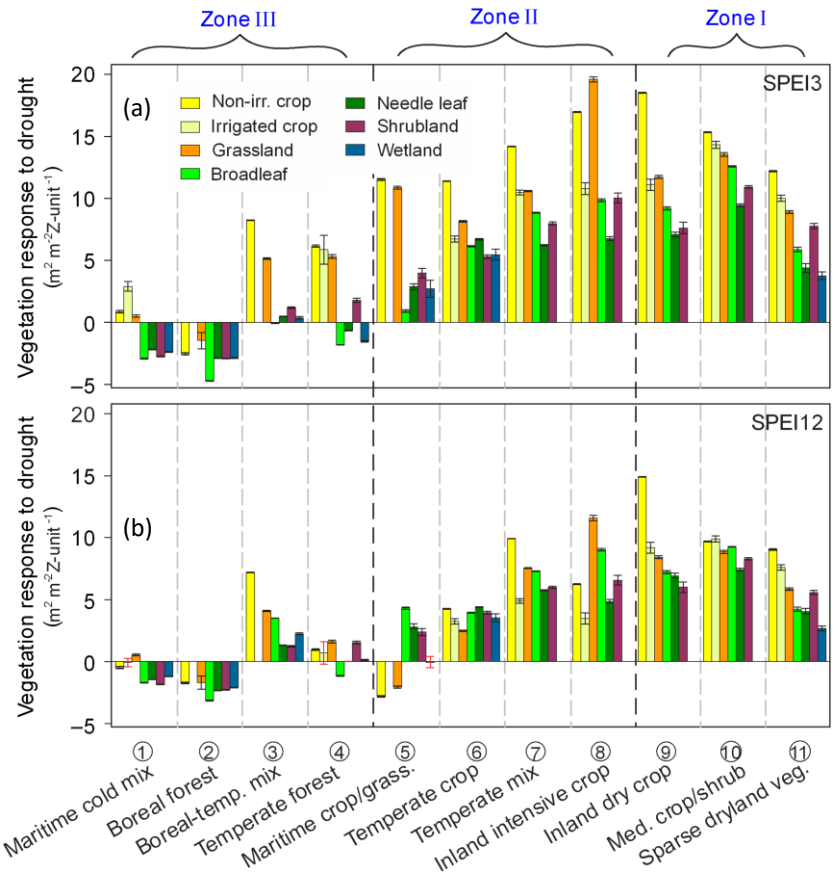

Figure 11. Average vegetation response to drought using (a) SPEI3 and (b) SPEI12 respectively in 11 drought-vegetation association classes and 7 vegetated land covers, determined from the meta-analysis of regression slopes of the pixels in each class. A positive value indicates vegetation productivity decreases with increase in drought intensity, and a negative indicates the opposite. Error bars denote the standard error of the mean responsivity, with red denoting insignificant (p>0.05).

scale droughts. The same land cover can have diverse drought responsivity depending on the vegetation-drought association class it belongs to (Figure 11).

The 11 vegetation-drought association classes can be grouped into three zones, based on their distinct plastic-rigid responses at different phenological stages. Zone I (classes ⑨–⑪): plants respond to drought with strong plasticity almost during the whole growing season. Zone II (classes ⑤–⑧): plants respond to drought with strong plasticity mainly at the end-of-season (EOS), but they also show rigid responses at the start-of-season (SOS). Zone III (classes ①–④): plants respond to drought with rigidity nearly during the whole growing season, with only weak insignificant plasticity at the EOS. The zonal transition classes ⑤ and ⑨ stand out with the responsivity characteristics of adjacent zones. Grassland and non-irrigated croplands in class ⑤ are plastic to short time-scale but rigid to long time-scale drought accumulation.

4. Discussion

The ability of plants to regulate their productivity with environmental changes, i.e. growth plasticity, is an important characteristic to survive under stress (Laitinen and Nikoloski 2018). Plasticity means reduced plant productivity during a drought but on the other hand means that plants can recover quickly during rehydration. Growth plasticity is advantageous when resources are abundant (Alpert and Simms 2002). Vicente-Serrano *et al.* (2013) already showed that global biomes have stronger growth plasticity to short time-scale than to long time-scale droughts. We used a satellite-derived indicator in this study and showed further that vegetation productivity has varied plasticity to drought stress over seasonal growing cycles, and the variation is related to aridity conditions and vegetation types.

Drought intensity increased across European biomes in the last two decades, however, the drying rate was small, and in general vegetation productivity did in fact increase. This increase in terrestrial vegetation productivity and greenness has been attributed to many factors like the CO_2 fertilization effect, nitrogen deposition, land use change, farming intensification, ecosystem restoration etc. (Chen et al. 2019; Zhu et al. 2016). We find that growing season drought intensified the most in western Russia, central and western European regions, and Sweden. Southern Europe, particularly the northern Mediterranean region, has experienced decreased drought intensity during the

growing season in the last two decades. Increasing drought intensity in Sweden might be attributed to temperature increase. Dai (2011) noted that Sweden had a drying trend when temperature change was included in PDSI computation, otherwise a wet trend predominated. Lloyd-Hughes and Saunders (2002) also showed that part of Sweden has a drying trend when using PDSI, and a wetting trend when using SPI. Our results extended those of Lloyd-Hughes and Saunders (2002) for the last century in Europe, and agree that the trend in European drought is generally small, but strong in specific regions. Lloyd-Hughes and Saunders (2002) also reported that some central and Eastern European countries and western Russia became drier, and parts of the northern Mediterranean region became wetter in the 20th century.

Our study used the high-resolution multi-source ensemble precipitation data MSWEP (Beck et al. 2019) and focused on the growing season period vegetation responses. We revealed more spatially detailed wetting tendencies in the northern Mediterranean regions, particularly the European highlands and alpine regions, which may explain the increased greening of the European Alps shown from 30m-resolution Landsat imagery (Rumpf *et al.* 2022). These wetting details may be concealed in drought trends from coarse data that show a pattern of north-wet and south-dry, as demonstrated by Dai (2011) when the temperature is constant. We also noticed that even ERA5-Land precipitation data also have high spatial resolution and similar inter-annual variations as other precipitation data, but the absolute precipitation values in ERA5-Land are much higher, which can obscure the variation AED caused by warming in SPEI estimation. That is, the warm-induced drying may not be properly reflected in SPEI when using ERA5-Land precipitation data.

We found that vegetation across European biomes can dynamically respond to drought late in the growing season (terminal droughts), and the drier the biome, the stronger the response. The later season growth plasticity (Class ⑤–⑧) to drought indicates that plants can adjust their growing processes according to water availability in general at the biome level, a strategy of plants to escape drought or to maximize growth if there is water. The strategy is comparable to that of leaf level, whereby plants shed old leaves under water stress or increase their lifespan if there is no resource shortage (Pinheiro and Chaves 2010; Reich *et al.* 1992).

With aridity increase (Class ⑨–⑪), vegetation growth plasticity to drought extends to the middle and the beginning of the growing season. The seasonal shift of plastic response to droughts across

biomes — from weak plasticity during the late season in humid biomes, to strong plasticity in subhumid biomes, and eventually to season-long strong plasticity in arid biomes — demonstrates a progressive plant reaction to water availability and adaptation to drought stress. That plants in humid and subhumid biomes have rigid responses to drought in the early season implies that they have no or weak adaptation to early spring droughts. Such rigidity also implies that plants may fail to recover with post-drought rehydration and therefore are vulnerable to severe droughts in spring.

The vegetation-drought associations across European biomes are co-determined by the geographical distribution of vegetated landcover types and aridity conditions. Vegetation productivity is significantly correlated to drought at a range of time-scales. The strongest correlation at a single time-scale cannot depict the complicated vegetation-drought relationship, particularly when using coarse climate data and pixels covering different herbaceous and woody plant types that respond differently to drought. To separately account for different responses of different vegetation types to various durations of water deficits, both short time-scale (e.g. SPEI3) and long time-scale (e.g. SPEI12) are needed. However, if short and long time-scale droughts are decoupled, as is the case for SPEI3 and SPEI12 in recent years, with more flash droughts (Christian et al. 2021), the overall vegetation productivity will fail to follow either drought indicator, complicating drought impacts on vegetation growth.

The out-of-sync response between time-scale-dependent drought extreme events and the anomalies of vegetation productivity in 2018 and 2019 leads to difficulties in generalizing drought impacts on vegetation. For example, in 2003 the European atmospheric drought intensity showed SPEI extremes at both 3- and 12-month time-scales, jointly forcing vegetation to the lowest productivity. However, in 2018–19, SPEI extremes on 3- and 12-month time-scales were reached one after the other, affecting shallow- and deep-rooted plants alternately, and although grassland and croplands suffered strong productivity decrease, there was no widespread exceptional reduction in vegetation productivity affecting all land covers.

5. Conclusions

- Over the last two decades, drought intensity has increased in central Europe, western Russia, and parts of Sweden, while it has decreased in the northern Mediterranean region.

- Vegetation responses to drought have divergent geographical distributions across Europe, closely related to regional vegetation types and aridity conditions.
- In arid biomes, plants are drought-adapted and have strong all-year plastic response to drought.
- In humid biomes, the vegetation drought response is rigid in general, only with more plastic responses toward the end of the growing season. More rigid responses are found at the beginning of the season in subhumid biomes.
- The time and place that plants have no drought adaptation and a rigid response to drought reveal high drought vulnerability, which should be considered in drought preparedness planning under the changing climate.

6. References

Abdi, A.M., Boke-Olén, N., Jin, H., Eklundh, L., Tagesson, T., Lehsten, V., & Ardö, J. (2019). First assessment of the plant phenology index (PPI) for estimating gross primary productivity in African semi-arid ecosystems. *International Journal of Applied Earth Observation and Geoinformation, 78*, 249-260

Allen, C.D., Macalady, A.K., Chenchouni, H., Bachelet, D., McDowell, N., Vennetier, M., Kitzberger, T., Rigling, A., Breshears, D.D., Hogg, E.H., Gonzalez, P., Fensham, R., Zhang, Z., Castro, J., Demidova, N., Lim, J.-H., Allard, G., Running, S.W., Semerci, A., & Cobb, N. (2010). A global overview of drought and heat-induced tree mortality reveals emerging climate change risks for forests. *Forest Ecology and Management, 259*, 660-684

Allen, R.G., Pereira, L.S., Raes, D., & Smith, M. (1998). *Crop evapotranspiration: guidelines for computing crop water requirements, FAO Irrigation and Drainage Paper No. 56*. FAO, Rome, Italy

Alpert, P., & Simms, E.L. (2002). The relative advantages of plasticity and fixity in different environments: when is it good for a plant to adjust? *Evolutionary Ecology, 16*, 285-297

Anderegg, W.R.L., Berry, J.A., Smith, D.D., Sperry, J.S., Anderegg, L.D.L., & Field, C.B. (2012). The roles of hydraulic and carbon stress in a widespread climate-induced forest die-off. *Proceedings of the National Academy of Sciences, 109*, 233-237

Andrea, T., Dario, M., Juan, A.N., Davide, B., Carmelo, C., Alfred, D.J., Chiara, D.C., Arthur, H.E., Willem, M., Diego, M., Marco, M., Jonathan, S., & Matteo, D.F. (2022). Drought in Europe July 2022. In. Publications Office of the European Union, Luxembourg, 2022

Bachmair, S., Tanguy, M., Hannaford, J., & Stahl, K. (2018). How well do meteorological indicators represent agricultural and forest drought across Europe? *Environmental Research Letters, 13*, 034042

Baena-González, E., Rolland, F., Thevelein, J.M., & Sheen, J. (2007). A central integrator of transcription networks in plant stress and energy signalling. *Nature, 448*, 938-942

Bastos, A., Fu, Z., Ciais, P., Friedlingstein, P., Sitch, S., Pongratz, J., Weber, U., Reichstein, M., Anthoni, P., Arneth, A., Haverd, V., Jain, A., Joetzjer, E., Knauer, J., Lienert, S., Loughran, T., McGuire, P.C., Obermeier, W., Padrón, R.S., Shi, H., Tian, H., Viovy, N., & Zaehle, S. (2020). Impacts of extreme summers on European ecosystems: a comparative analysis of 2003, 2010 and 2018. *Philosophical Transactions of the Royal Society B: Biological Sciences, 375*, 20190507

Basu, S., Ramegowda, V., Kumar, A., & Pereira, A. (2016). Plant adaptation to drought stress. *F1000Research, 5*, F1000 Faculty Rev-1554

Beck, H.E., Wood, E.F., Pan, M., Fisher, C.K., Miralles, D.G., van Dijk, A.I.J.M., McVicar, T.R., & Adler, R.F. (2019). MSWEP V2 Global 3-Hourly 0.1° Precipitation: Methodology and Quantitative Assessment. *Bulletin of the American Meteorological Society, 100*, 473-500

Becker, B.J., & Wu, M.-J. (2007). The Synthesis of Regression Slopes in Meta-Analysis. *Statistical Science, 22*, 414-429

Bohnert, H.J., Nelson, D.E., & Jensen, R.G. (1995). Adaptations to Environmental Stresses. *The Plant Cell, 7*, 1099-1111

Bongers, F.J., Olmo, M., Lopez-Iglesias, B., Anten, N.P.R., & Villar, R. (2017). Drought responses, phenotypic plasticity and survival of Mediterranean species in two different microclimatic sites. *Plant Biology, 19*, 386-395

Büntgen, U., Urban, O., Krusic, P.J., Rybníček, M., Kolář, T., Kyncl, T., Ač, A., Koňasová, E., Čáslavský, J., Esper, J., Wagner, S., Saurer, M., Tegel, W., Dobrovolný, P., Cherubini, P., Reinig, F., & Trnka, M. (2021). Recent European drought extremes beyond Common Era background variability. *Nature Geoscience, 14*, 190-196

Camarero, J.J., Gazol, A., Sangüesa-Barreda, G., Oliva, J., & Vicente-Serrano, S.M. (2015). To die or not to die: early warnings of tree dieback in response to a severe drought. *Journal of Ecology, 103*, 44-57

Cammalleri, C., Naumann, G., Mentaschi, L., Formetta, G., Forzieri, G., Gosling, S., Bisselink, B., De Roo, A., & Feyen, L. (2020). Global warming and drought impacts in the EU. In, *JRC Technical report*. Luxembourg: Publications Office of the European Union

Choat, B., Jansen, S., Brodribb, T.J., Cochard, H., Delzon, S., Bhaskar, R., Bucci, S.J., Feild, T.S., Gleason, S.M., Hacke, U.G., Jacobsen, A.L., Lens, F., Maherali, H., Martínez-Vilalta, J., Mayr, S., Mencuccini, M., Mitchell, P.J., Nardini, A., Pittermann, J., Pratt, R.B., Sperry, J.S., Westoby, M., Wright, I.J., & Zanne, A.E. (2012). Global convergence in the vulnerability of forests to drought. *Nature, 491*, 752-755

Christopoulou, A., Sazeides, C.I., & Fyllas, N.M. (2021). Size-mediated effects of climate on tree growth and mortality in Mediterranean Brutia pine forests. *Science of the Total Environment*, 151463

Ciais, P., Reichstein, M., Viovy, N., Granier, A., Ogée, J., Allard, V., Aubinet, M., Buchmann, N., Bernhofer, C., Carrara, A., Chevallier, F., De Noblet, N., Friend, A.D., Friedlingstein, P., Grünwald, T., Heinesch, B., Keronen, P., Knohl, A., Krinner, G., Loustau, D., Manca, G., Matteucci, G., Miglietta, F., Ourcival, J.M., Papale, D., Pilegaard, K., Rambal, S., Seufert, G., Soussana, J.F., Sanz, M.J., Schulze, E.D., Vesala, T., & Valentini, R. (2005). Europe-wide reduction in primary productivity caused by the heat and drought in 2003. *Nature, 437*, 529

Cruz de Carvalho, M.H. (2008). Drought stress and reactive oxygen species: Production, scavenging and signaling. *Plant Signaling & Behavior, 3*, 156-165

Csermely, P. (2015). Plasticity-rigidity cycles: A general adaptation mechanism. *arXiv preprint arXiv:1511.01239*

Dai, A. (2011). Characteristics and trends in various forms of the Palmer Drought Severity Index during 1900–2008. *Journal of Geophysical Research: Atmospheres, 116*

Deng, Y., Wang, X., Wang, K., Ciais, P., Tang, S., Jin, L., Li, L., & Piao, S. (2021). Responses of vegetation greenness and carbon cycle to extreme droughts in China. *Agricultural and Forest Meteorology, 298-299*, 108307

Douville, H., Raghavan, K., Renwick, J., Allan, R.P., Arias, P.A., Cerezo-Mota, M.B.R., Cherchi, A., Gan, T.Y., Gergis, J., Jiang, D., Khan, A., Rosenfeld, W.P.M.D., Tierney, J., & Zolina, O. (2021). Water Cycle Changes. In V. Masson-Delmotte, P. Zhai, A. Pirani, S.L. Connors, C. Péan, S. Berger, N. Caud, Y. Chen, L. Goldfarb, M.I. Gomis, M. Huang, K. Leitzell, E. Lonnoy, J.B.R. Matthews, T.K. Maycock, T. Waterfield, O. Yelekçi, R. Yu, & B. Zhou (Eds.), *Climate Change 2021: The Physical Science Basis. Contribution of Working Group I to the Sixth Assessment Report of the Intergovernmental Panel on Climate Change*

Dracup, J.A., Lee, K.S., & Paulson Jr., E.G. (1980). On the definition of droughts. *Water Resources Research, 16*, 297-302

EEA (2021). Corine land cover user manual. In. Copenhagen: European Union, Copernicus Land Monitoring Service, European Environment Agency (EEA)

EEA (2022). MR-VPP Product Plant Phenology Index and VPP parameters, issue 1.0. In E. Itvis (Ed.). Copenhagen, Denmark

Folke, C. (2006). Resilience: The emergence of a perspective for social–ecological systems analyses. *Global Environmental Change, 16*, 253-267

García-Herrera, R., Garrido-Perez, J.M., Barriopedro, D., Ordóñez, C., Vicente-Serrano, S.M., Nieto, R., Gimeno, L., Sorí, R., & Yiou, P. (2019). The European 2016/17 Drought. *Journal of Climate, 32*, 3169-3187

Gray, C., Ma, A., McLaughlin, O., Petit, S., Woodward, G., & Bohan, D.A. (2021). Ecological plasticity governs ecosystem services in multilayer networks. *Communications Biology, 4*, 75

Hartmann, H., Moura, C.F., Anderegg, W.R.L., Ruehr, N.K., Salmon, Y., Allen, C.D., Arndt, S.K., Breshears, D.D., Davi, H., Galbraith, D., Ruthrof, K.X., Wunder, J., Adams, H.D., Bloemen, J., Cailleret, M., Cobb, R., Gessler, A., Grams, T.E.E., Jansen, S., Kautz, M., Lloret, F., & O'Brien, M. (2018). Research frontiers for improving our understanding of drought-induced tree and forest mortality. *New Phytologist, 218*, 15-28

Holling, C.S., & Meffe, G.K. (1996). Command and Control and the Pathology of Natural Resource Management. *Conservation Biology, 10*, 328-337

Horion, S., Carrão, H., Singleton, A., Barbosa, P., & Vogt, J. (2012). JRC experience on the development of drought information systems. Europe, Africa and Latin America. EUR 25235 EN. Publications Office of the European Union, Luxembourg. In

Huang, W., & Wang, H. (2021). Drought and intensified agriculture enhanced vegetation growth in the central Pearl River Basin of China. *Agricultural Water Management, 256*, 107077

Huffman, G.J., Stocker, E.F., Bolvin, D.T., Nelkin, E.J., & Tan, J. (2019). GPM IMERG Final Precipitation L3 Half Hourly 0.1 degree x 0.1 degree V06, Greenbelt, MD, Goddard Earth Sciences Data and Information Services Center (GES DISC),Accessed: [2023-03-10

Date]. In

IPCC (2021). Climate Change 2021: The Physical Science Basis. Contribution of Working Group I to the Sixth Assessment Report of the Intergovernmental Panel on Climate Change. In V. Masson-Delmotte, P. Zhai, A. Pirani, S.L. Connors, C. Péan, S. Berger, N. Caud, Y. Chen, L. Goldfarb, M.I. Gomis, M. Huang, K. Leitzell, E. Lonnoy, J.B.R. Matthews, T.K. Maycock, T. Waterfield, O. Yelekçi, R. Yu, & B. Zhou (Eds.)

Ivits, E., Horion, S., Erhard, M., & Fensholt, R. (2016). Assessing European ecosystem stability to drought in the vegetation growing season. *Global Ecology and Biogeography, 25*, 1131-1143

Ivits, E., Horion, S., Fensholt, R., & Cherlet, M. (2014). Drought footprint on European ecosystems between 1999 and 2010 assessed by remotely sensed vegetation phenology and productivity. *Global Change Biology, 20*, 581-593

Jin, H., & Eklundh, L. (2014). A physically based vegetation index for improved monitoring of plant phenology. *Remote Sensing of Environment, 152*, 512-525

Jin, H., Jönsson, A.M., Bolmgren, K., Langvall, O., & Eklundh, L. (2017). Disentangling remotely-sensed plant phenology and snow seasonality at northern Europe using MODIS and the plant phenology index. *Remote Sensing of Environment, 198*, 203-212

Jin, H., Jönsson, A.M., Olsson, C., Lindström, J., Jönsson, P., & Eklundh, L. (2019). New satellite-based estimates show significant trends in spring phenology and complex sensitivities to temperature and precipitation at northern European latitudes. *International Journal of Biometeorology, 63*, 763–775

Jönsson, P., & Eklundh, L. (2004). TIMESAT—a program for analyzing time-series of satellite sensor data. *Computers & Geosciences, 30*, 833-845

Junttila, S., Ardö, J., Cai, Z., Jin, H., Kljun, N., Klemedtsson, L., Krasnova, A., Lange, H., Lindroth, A., Mölder, M., Noe, S.M., Tagesson, T., Vestin, P., Weslien, P., & Eklundh, L. (2023). Estimating local-scale forest GPP in Northern Europe using Sentinel-2: Model comparisons with LUE, APAR, the plant phenology index, and a light response function. *Science of Remote Sensing, 7*, 100075

Khoury, S., & Coomes, D.A. (2020). Resilience of Spanish forests to recent droughts and climate change. *Global Change Biology, 26*, 7079-7098

Laitinen, R.A.E., & Nikoloski, Z. (2018). Genetic basis of plasticity in plants. *Journal of Experimental Botany, 70*, 739-745

Lawal, S., Hewitson, B., Egbebiyi, T.S., & Adesuyi, A. (2021). On the suitability of using vegetation indices to monitor the response of Africa's terrestrial ecoregions to drought. *Science of The Total Environment, 792*, 148282

Li, X., & Xiao, J. (2019). Mapping Photosynthesis Solely from Solar-Induced Chlorophyll Fluorescence: A Global, Fine-Resolution Dataset of Gross Primary Production Derived from OCO-2. *Remote Sensing, 11*, 2563

Lindroth, A., Holst, J., Linderson, M.-L., Aurela, M., Biermann, T., Heliasz, M., Chi, J., Ibrom, A., Kolari, P., Klemedtsson, L., Krasnova, A., Laurila, T., Lehner, I., Lohila, A., Mammarella, I., Mölder, M., Löfvenius, M.O., Peichl, M., Pilegaard, K., Soosaar, K., Vesala, T., Vestin, P., Weslien, P., & Nilsson, M. (2020). Effects of drought and meteorological forcing on carbon and water fluxes in Nordic forests during the dry summer of 2018. *Philosophical Transactions of the Royal Society B: Biological Sciences, 375*, 20190516

Lloret, F., Keeling, E.G., & Sala, A. (2011). Components of tree resilience: effects of successive low-growth episodes in old ponderosa pine forests. *Oikos, 120*, 1909-1920

Maaten, L.v.d., & Hinton, G. (2008). Visualizing Data using t-SNE. *Journal of Machine Learning Research, 9*, 2579–2605

Marchin, R.M., Backes, D., Ossola, A., Leishman, M.R., Tjoelker, M.G., & Ellsworth, D.S. (2022). Extreme heat increases stomatal conductance and drought-induced mortality risk in vulnerable plant species. *Global Change Biology, 28*, 1133-1146

McDowell, N., Pockman, W.T., Allen, C.D., Breshears, D.D., Cobb, N., Kolb, T., Plaut, J., Sperry, J., West, A., Williams, D.G., & Yepez, E.A. (2008). Mechanisms of plant survival and mortality during drought: why do some plants survive while others succumb to drought? *New Phytologist, 178*, 719-739

McDowell, N.G., Beerling, D.J., Breshears, D.D., Fisher, R.A., Raffa, K.F., & Stitt, M. (2011). The interdependence of mechanisms underlying climate-driven vegetation mortality. *Trends in Ecology & Evolution, 26*, 523-532

Mishra, A.K., & Singh, V.P. (2010). A review of drought concepts. *Journal of Hydrology, 391*, 202-216

Myneni, R.B., Keeling, C.D., Tucker, C.J., Asrar, G., & Nemani, R.R. (1997). Increased plant growth in the northern high latitudes from 1981 to 1991. *Nature, 386*, 698-702

Naumann, G., Cammalleri, C., Mentaschi, L., & Feyen, L. (2021). Increased economic drought impacts in Europe with anthropogenic warming. *Nature Climate Change, 11*, 485-491

Nicotra, A.B., Atkin, O.K., Bonser, S.P., Davidson, A.M., Finnegan, E.J., Mathesius, U., Poot, P., Purugganan, M.D., Richards, C.L., Valladares, F., & van Kleunen, M. (2010). Plant phenotypic plasticity in a changing climate. *Trends in Plant Science, 15*, 684-692

Passioura, J.B. (2002). Environmental biology and crop improvement. *Functional Plant Biology, 29*, 537-546

Pellizzari, E., Camarero, J.J., Gazol, A., Granda, E., Shetti, R., Wilmking, M., Moiseev, P., Pividori, M., & Carrer, M. (2017). Diverging shrub and tree growth from the Polar to the Mediterranean biomes across the European continent. *Global Change Biology, 23*, 3169-3180

Pinheiro, C., & Chaves, M.M. (2010). Photosynthesis and drought: can we make metabolic connections from available data? *Journal of Experimental Botany, 62*, 869-882

Reich, P.B., Walters, M.B., & Ellsworth, D.S. (1992). Leaf Life-Span in Relation to Leaf, Plant, and Stand Characteristics among Diverse Ecosystems. *Ecological Monographs, 62*, 365-392

Reinhart, V., Fonte, C.C., Hoffmann, P., Bechtel, B., Rechid, D., & Boehner, J. (2021). Comparison of ESA climate change initiative land cover to CORINE land cover over Eastern Europe and the Baltic States from a regional climate modeling perspective. *International Journal of Applied Earth Observation and Geoinformation, 94*, 102221

Rumpf, S.B., Gravey, M., Brönnimann, O., Luoto, M., Cianfrani, C., Mariethoz, G., & Guisan, A. (2022). From white to green: Snow cover loss and increased vegetation productivity in the European Alps. *Science, 376*, 1119-1122

Running, S.W., Nemani, R.R., Heinsch, F.A., Zhao, M., Reeves, M., & Hashimoto, H. (2004). A Continuous Satellite-Derived Measure of Global Terrestrial Primary Production. *BioScience, 54*, 547-560

Sánchez-Salguero, R., Camarero, J.J., Rozas, V., Génova, M., Olano, J.M., Arzac, A., Gazol, A., Caminero, L., Tejedor, E., de Luis, M., & Linares, J.C. (2018). Resist, recover or both? Growth plasticity in response to drought is geographically structured and linked to intraspecific variability in Pinus pinaster. *Journal of Biogeography, 45*, 1126-1139

Senf, C., Buras, A., Zang, C.S., Rammig, A., & Seidl, R. (2020). Excess forest mortality is consistently linked to drought across Europe. *Nature Communications, 11*, 6200

Shinozaki, K., & Yamaguchi-Shinozaki, K. (2006). Gene networks involved in drought stress response and tolerance. *Journal of Experimental Botany, 58*, 221-227

Spinoni, J., Naumann, G., & Vogt, J.V. (2017). Pan-European seasonal trends and recent changes of drought frequency and severity. *Global and Planetary Change, 148*, 113-130

Strosser, P., Dworak, T., Garzon Delvaux, P., Berglund, M., Schmidt, G., Mysiak, J., Kossida, M., Iacovides, I., & Ashton, V. (2012). Final Report Gap Analysis of the Water Scarcity and Droughts Policy in the EU. In (p. 206): European Commission

Sun, Q., Miao, C., Duan, Q., Ashouri, H., Sorooshian, S., & Hsu, K.-L. (2018). A Review of Global Precipitation Data Sets: Data Sources, Estimation, and Intercomparisons. *Reviews of Geophysics, 56*, 79-107

Tagesson, T., Tian, F., Schurgers, G., Horion, S., Scholes, R., Ahlström, A., Ardö, J., Moreno, A., Madani, N., Olin, S., & Fensholt, R. (2021). A physiology-based Earth observation model indicates stagnation in the global gross primary production during recent decades. *Global Change Biology, 27*, 836-854

Tian, F., Cai, Z., Jin, H., Hufkens, K., Scheifinger, H., Tagesson, T., Smets, B., Van Hoolst, R., Bonte, K., Ivits, E., Tong, X., Ardö, J., & Eklundh, L. (2021). Calibrating vegetation phenology from Sentinel-2 using eddy covariance, PhenoCam, and PEP725 networks across Europe. *Remote Sensing of Environment, 260*, 112456

Tian, L., Yuan, S., & Quiring, S.M. (2018). Evaluation of six indices for monitoring agricultural drought in the south-central United States. *Agricultural and Forest Meteorology, 249*, 107-119

Van Loon, A.F. (2015). Hydrological drought explained. *WIREs Water, 2*, 359-392

Van Loon, A.F., Gleeson, T., Clark, J., Van Dijk, A.I.J.M., Stahl, K., Hannaford, J., Di Baldassarre, G., Teuling, A.J., Tallaksen, L.M., Uijlenhoet, R., Hannah, D.M., Sheffield, J., Svoboda, M., Verbeiren, B., Wagener, T., Rangecroft, S., Wanders, N., & Van Lanen, H.A.J. (2016). Drought in the Anthropocene. *Nature Geoscience, 9*, 89-91

Vicente-Serrano, S.M., Beguería, S., & López-Moreno, J.I. (2010). A Multiscalar Drought Index Sensitive to Global Warming: The Standardized Precipitation Evapotranspiration Index. *Journal of Climate, 23*, 1696-1718

Vicente-Serrano, S.M., Gouveia, C., Camarero, J.J., Beguería, S., Trigo, R., López-Moreno, J.I., Azorín-Molina, C., Pasho, E., Lorenzo-Lacruz, J., Revuelto, J., Morán-Tejeda, E., & Sanchez-Lorenzo, A. (2013). Response of vegetation to drought time-scales across global land biomes. *Proceedings of the National Academy of Sciences, 110*, 52-57

Vicente-Serrano, S.M., Quiring, S.M., Peña-Gallardo, M., Yuan, S., & Domínguez-Castro, F. (2020). A review of environmental droughts: Increased risk under global warming? *Earth-Science Reviews, 201*, 102953

Wang, H., Vicente-serrano, S.M., Tao, F., Zhang, X., Wang, P., Zhang, C., Chen, Y., Zhu, D., & Kenawy, A.E. (2016). Monitoring winter wheat drought threat in Northern China using multiple climate-based drought indices and soil moisture during 2000–2013. *Agricultural and Forest Meteorology, 228-229*, 1-12

West, H., Quinn, N., & Horswell, M. (2019). Remote sensing for drought monitoring & impact assessment: Progress, past challenges and future opportunities. *Remote Sensing of Environment, 232*, 111291

Zhong, S., Sun, Z., & Di, L. (2021). Characteristics of vegetation response to drought in the CONUS based on long-term remote sensing and meteorological data. *Ecological Indicators, 127*, 107767

Zhu, Z., Bi, J., Pan, Y., Ganguly, S., Anav, A., Xu, L., Samanta, A., Piao, S., Nemani, R., & Myneni, R. (2013). Global Data Sets of Vegetation Leaf Area Index (LAI)3g and Fraction of Photosynthetically Active Radiation (FPAR)3g Derived from Global Inventory Modeling and Mapping Studies (GIMMS) Normalized Difference Vegetation Index (NDVI3g) for the Period 1981 to 2011. *Remote Sensing, 5*, 927-948

Supplementary material

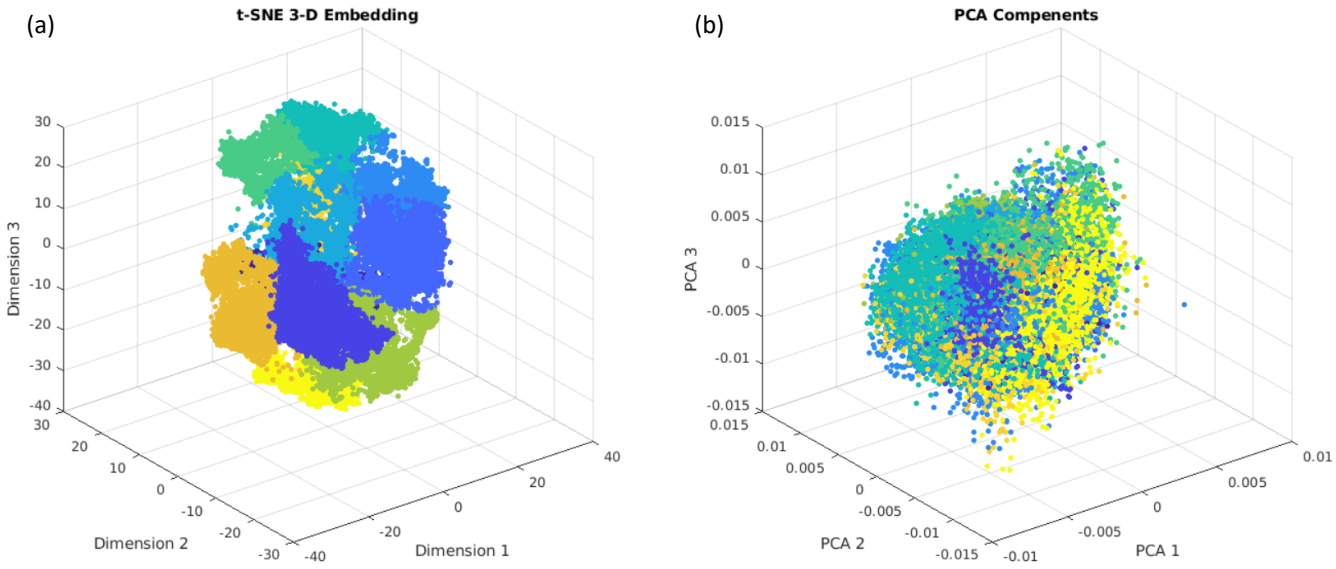

Figure S1. Comparison of clustering (a) using t-distributed stochastic neighbor embedding (t-SNE) and (b) principle component analysis (PCA)

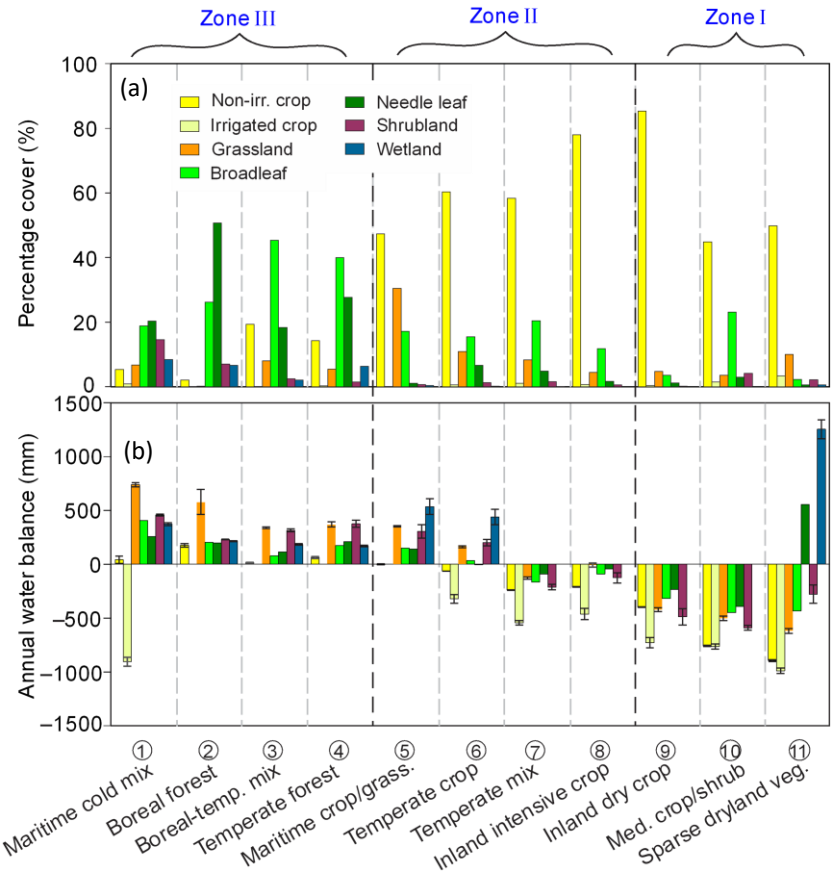

Figure S2. (a) Spatial percentage distribution of main 7 land cover types and (b) their average annual water balance (P-AED) of 11 vegetation-drought association classes in Europe.